Journal of Molecular Graphics and Modelling 42 (2013) 60–72

Contents lists available at SciVerse ScienceDirect

Journal of Molecular Graphics and Modelling

journal homepage: www.elsevier.com/locate/JMGM

A3 adenosine receptor: Homology modeling and 3D-QSAR studies

Anna Maria Almerico*, Marco Tutone, Licia Pantano, Antonino Lauria

Dipartimento di Scienze e Tecnologie Biologiche, Chimiche e Farmaceutiche (STEBICEF) – Sezione di Chimica Farmaceutica e Biologica, Università degli Studi di Palermo, Via Archirafi 32, 90123 Palermo, Italy

ARTICLE INFO

Article history:
Accepted 7 March 2013
Available online 19 March 2013

Keywords:
A3 Receptor
Homology modelling
Molecular dynamics simulation,
Pharmacophores

ABSTRACT

Adenosine receptors (AR) belong to the superfamily of G-protein-coupled receptors (GPCRs). They are divided into four subtypes (A1, A2A, A2B, and A3) and can be distinguished on the basis of their distinct molecular structures, distinct tissues distribution, and selectivity for adenosine analogs. The hA3R, the most recently identified adenosine receptor, is involved in a variety of intracellular signaling pathways and physiological functions. Expression of hA3R was reported to be elevated in cancerous tissues and A3 antagonists could be proposed for therapeutic treatments of tumor. By using the crystal structure of hA2A adenosine receptor, recently published, we were able to obtain a model for A3R, further optimized using nanosecond scale molecular dynamics simulation. One hundred twenty two active and selective compounds were docked into this model and used as training set to generate pharmacophore models. These last address the prevalent features to be used for the search of new inhibitors. Therefore, it was employed as template to screen the ZINC database in the attempt to find new potent and selective human A3R antagonists. Our theoretical model of hA3 adenosine receptor was used to evaluate and quantify the structure-activity relationship of known antagonists. Moreover the obtained 3D-QSAR model allowed to identify new potential inhibitors.

1. Introduction

The adenosine class of heterotrimeric guanine nucleotide-binding protein (G-protein) coupled receptors (GPCRs) mediates the important role of extracellular adenosine in many physiological processes. Adenosine is an ubiquitous neuromodulator that acts by stimulating four cell surface receptors (A1, A2A, A2B, A3), all being part of the huge family of the GPCRs. These receptors are widely distributed throughout the tissues. A2A and A2B receptors are coupled to adenylate cyclase activity, and their stimulation increases the intracellular cyclic adenosine monophosphate (cAMP) concentration, while A1 and A3 receptor stimulation decreases cAMP concentration and raises intracellular Ca^{2+} levels by a pathway involving phospholipase C (PLC) activation (Fig. 1) [1,2].

The A3R is involved in the control of the cell cycle and inhibition of tumour growth both in vitro and in vivo [3]. In fact adenosine A3 receptors have been demonstrated to be more highly expressed in tumours than in healthy cells, suggesting a role for A3R as a tumour marker [4].

Since many years our research group has been interested in developing molecular modelling techniques and QSAR/QSPR methodologies on several targets involved in carcinogenic processes [5–16]. In connection with these studies and although this point is strongly debated, in the present work we explored the role of A3R antagonists that could be used or provide an opportunity for the generation of novel compounds as potential chemotherapeutic agents.

All adenosine receptors have in common a core domain consisting of seven transmembrane helices (TM1–TM7), with each TM composed of 20–27 amino acids, connected by three intracellular (IL1–IL3) and three extracellular loops (EL1–EL3). The N-terminus is located at the extracellular side of the cell and often contains one or more glycosylation sites. The C-terminus is located intracellularly and contains phosphorylation and palmitoylation sites, which are involved in regulation of receptor desensitization and internalization [17].

All adenosine receptors, with the exception of the A2AR, contain a palmitoylation site near the C-terminus. The A2AR is the only subtype with an extraordinary long C-terminus [18]. All of them are glycosylated on the second extracellular loop, although glycosylation does not appear to influence ligand binding. The third intracellular loop and/or the C-terminus are involved in coupling the adenosine receptors to G-proteins.

The A1, A2B, and A3 receptors are very similar in regard to the number of amino acids composing their primary structure, the human homologs consist of 326, 328, and 318 amino acid residues, respectively. Conversely, the human A2A is composed by

* Corresponding author. Tel.: +39 0916161606/09123896804; fax: +39 09123860854.
E-mail address: annamaria.almerico@unipa.it (A.M. Almerico).

1093-3263/$ – see front matter © 2013 Elsevier Inc. All rights reserved.
http://dx.doi.org/10.1016/j.jmgm.2013.03.001

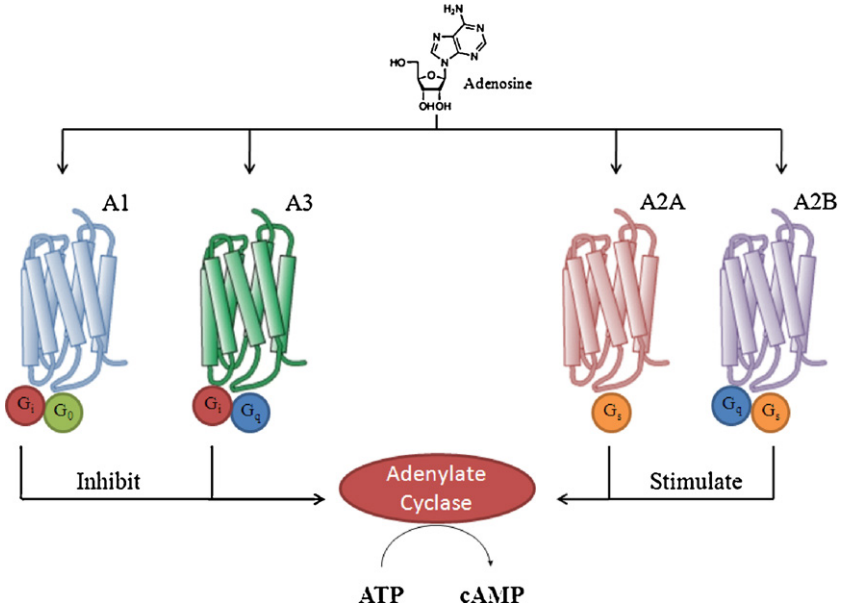

Fig. 1. Adenosine class of heterotrimeric guanine nucleotide-binding protein coupled receptors.

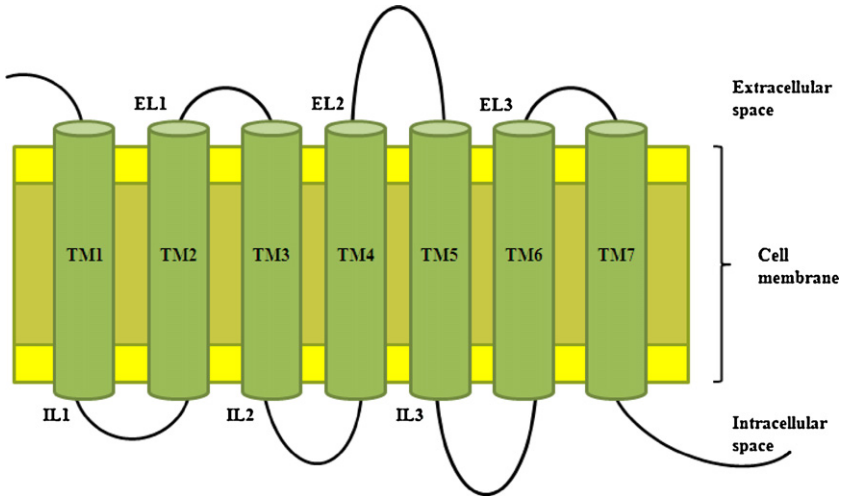

Fig. 2. Secondary structure of A3R.

409 amino acids. The human A1R and human A3R display 46.5% overall sequence identity at the amino acid level, while the human A2AR and human A2BR are 46.6% identical (Table 1).

2. Results and discussion

Homology modeling is a theoretical method that is used to predict the structure of a sequence with an accurancy that is comparable to the best results achieved experimentally. The A3 adenosine receptor has 318 amino acids and contains 7 TM helices connected by three intracellular and three extracellular loops (Figs. 2 and 3).

Table 1
Percentage of sequence identity.

	A2A	A2B	A3
A1	38.3	44.0	46.5
A2A		46.6	31.0
A2B			35.7

For many years rhodopsin had represented the only structural information available for GPCRs. The first resolved structure of rhodopsin was published in 2000 by Palezewski et al. [19] and it had been broadly used as template [20]. In 2008 the crystal structure of the human A2A adenosine receptor in complex with a selective antagonist ZM241385 (PDB ID: 3EML) was resolved [21] (Fig. 4).

Crystallographic model reveals features different from previously reported GPCR structures (Table 2). The organization of the extracellular loops is markedly different from β1AR, β2AR and bovine rhodopsin [22–24] (Fig. 5).

Furthermore ZM241385 binds A2A in conformation perpendicular to the plane of the membrane and co-linear with transmembrane helix VII, interacting with both EL2 and EL3. Finally, the binding pocket of the A2A adenosine receptor results very close to helices VI and VII and only limited interactions with helices III and V are allowed.

These structural information are the basis for our homology modeling of hA3R adenosine receptor. The A3 protein sequence was collected from the Swiss-Prot Protein Database (P33765) [25,26]. The A2A adenosine receptor can be considered the best template

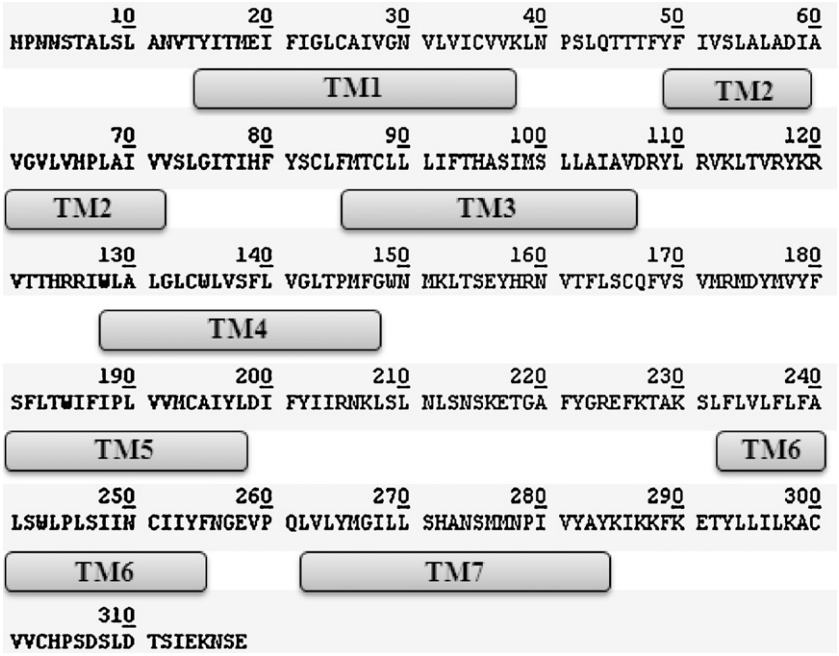

Fig. 3. Schematic representation of the human A3 adenosine receptor.

Table 2
Reported GPCR structures.

Protein or complex	PDB code	Resolution	Species
Rhodopsin	1F88, 1GZM, 1HZX, 1L9H, **1U19**, 2G87, 2HPY, 2I35, 2I36, 2I37, 2J4Y, 2PED, 2X72, 3C9L, 3CM9, 3CAP, 3DQB, 3OAX, 3PQR, 3PXO	2.2–4.15 Å	Bovine
β1-Adrenergic receptor	**2VT4**, 2Y00, 2Y01, 2Y02, 2Y03, 2Y04, 2YCW, 2YCX, 2YCZ, 2YCY, 4AMI, 4AMJ	2.5–3.05 Å	Turkey
β2-Adrenergic receptor	2R4H, 2R4S, **2RH1**, 3D4S, 3KJ6, 3NY8, 3NY9, 3NYA, 3PDS	2.4–3.5 Å	Human
Adenosine A2A receptor	**3EML**, 3QAK	2.6–2.7 Å	Human

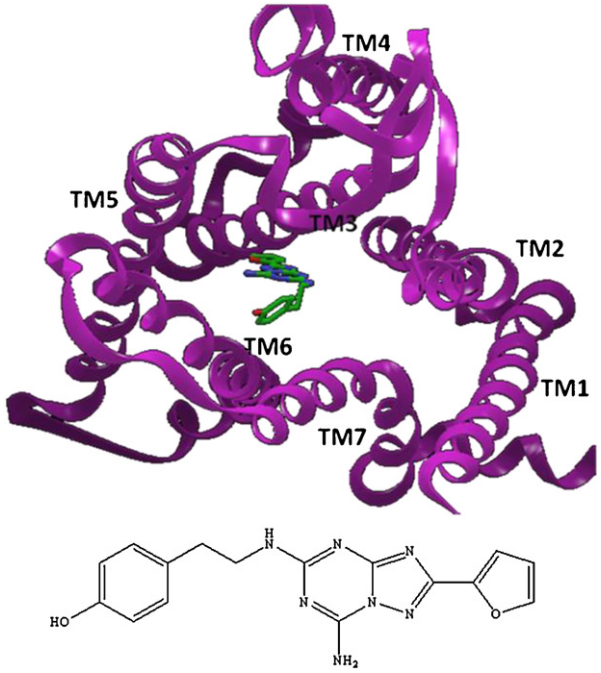

Fig. 4. Crystal structure of the human A2A adenosine receptor in complex with ZM241385 (chemical structure of which is reported below; top-down orientation).

for homology modeling according to the percentage identity of the aligned sequence. Identity increases from bovine rhodopsin to hA2A adenosine receptor. The increase is even higher when comparing only TM regions and if N- and C-terminus are not taken into consideration (Table 3).

Two different models of hA3R were generated by LOMETS [27] using the bovine rhodopsin (PDB ID: 1U19) and the hA2A adenosine receptor (PDB ID: 3EML) as templates (Fig. 6).

As it is seen from the RMSD values of the aligned models, the main differences among the two models are found within EL2 and IL3 loops (Table 4). In particular EL2 belongs to the binding pocket and interact with ligand. In the model built using hA2A as template,

Table 3
Percentage of sequence identity.

		Rhodopsin	hA2A
All	hA1	15.3	38.3
	hA2A	14.5	100
	hA2B	19.5	46.6
	hA3	14.4	31
TM regions	hA1	15.7	60.8
	hA2A	23.2	100
	hA2B	22	68.6
	hA3	19.3	50.3
All except N and C-terminus	hA1	16.4	51.7
	hA2A	21.2	100
	hA2B	22.9	61.6
	hA3	16	41.9

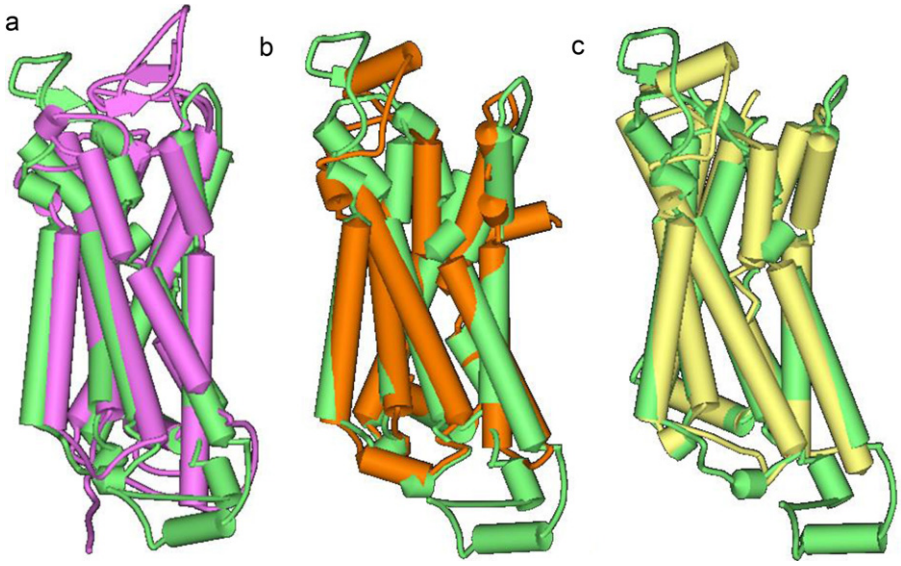

Fig. 5. Superimposition of A2A adenosine receptor (green) with bovine rhodopsin (purple) (a), β1AR (orange) (b), β2AR (yellow) (c). (For interpretation of the references to color in text, the reader is referred to the web version of the article.)

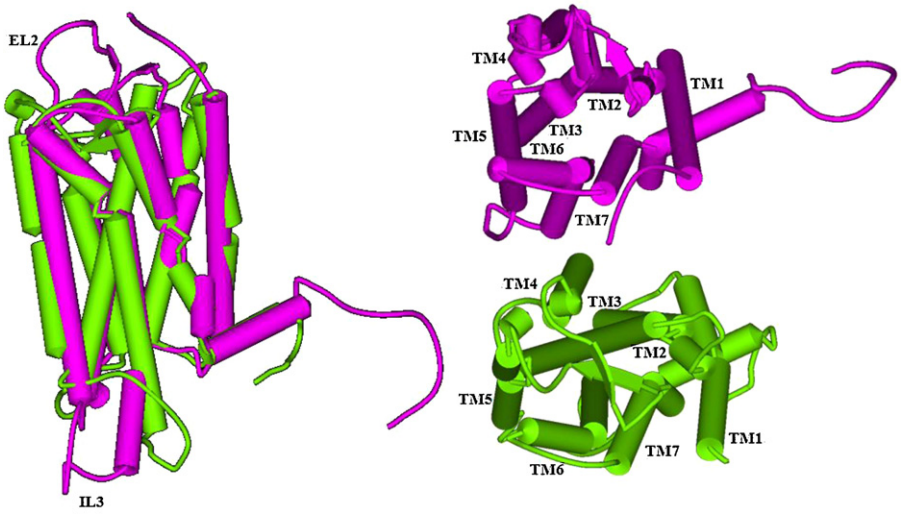

Fig. 6. Superposition of hA3 models built using rhodopsin (green) and hA2A (purple) as templates.

the binding pocket is open to extracellular side and closer to TM6 and TM7.

Obviously, as expected, the more suitable model was derived from the human receptor, therefore by using the new structure of hA2A adenosine receptor it was possible to improve modelization of A3 adenosine receptor. Obtained model was refined using MoodLoop [28], and was ranked on QMEAN server [29]. QMEAN is a composite scoring function which is able to derive both global (i.e. for the entire structure) and local (i.e. per residue) error estimates on the basis of one single model. It takes into account torsion, solvation, secondary structure. The model created using template 3EML had higher QMEAN score (0.47) than the one generated using template 1U19 (0.40). The overall stereochemical quality of the model was assessed by PROCHECK [30] and the validation of the structure was performed by inspecting the psi/phi Ramachandran plot (Fig. 7).

The Ramachandran plot showed 94.3% of the residues in the most favorable region, 5.4% in the allowed region, 0.3% in the generously allowed region. This result revealed that the obtained model is reliable and of good quality.

Homology models represent a rigid conformation of a protein, but proteins are dynamic and show rapid, small-scale structural fluctuation [31]. Obtained model supposed to be antagonist-like state of A3 receptor and it can exist in more than one conformational state. So a 20 ns molecular dynamics simulation in a lipid

Table 4
RMSD of the aligned hA3 adenosine receptor models built using A2A and rhodopsin.

	RMSD
Backbone	7.08
IL1	1.18
IL2	3.01
IL3	6.26
EL1	3.47
EL2	6.74
EL3	1.36
TM1	0.70
TM2	1.37
TM3	0.98
TM4	1.39
TM5	1.03
TM6	0.75
TM7	0.93

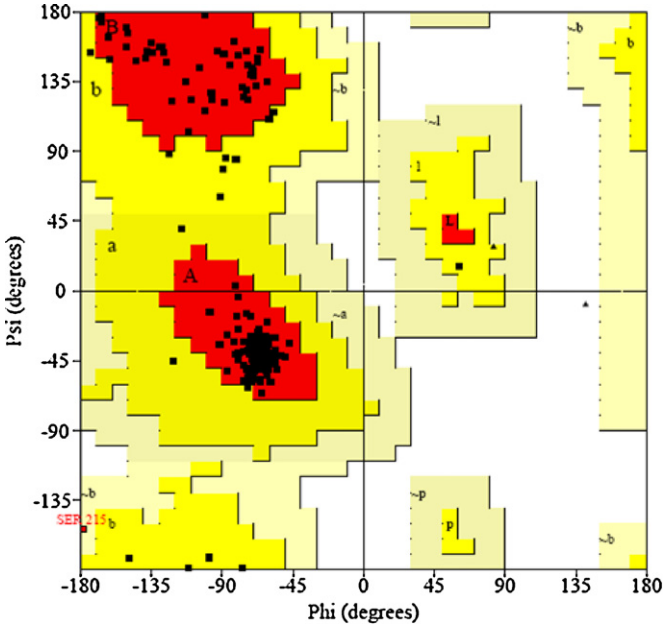

Fig. 7. Ramachandran plot of obtained model.

bilayer was performed to explain conformational flexibility and structural stability using the program DESMOND [32]. The structural changes and dynamic behavior were analyzed by calculating the RMSD of the TMs (Fig. 8) and loops (Fig. 9) backbone in function of time (ns).

Very short loop, such as IL1, EL1, and EL3, have low values of RMSD, together with longer loop like IL2. N-term and C-term are very flexible, probably due to the fact that are more exposed. Longer loop like IL3 and EL2 are more flexible (Fig. 10). TMs show that the conformation is more stable through 20 ns of simulation. The RMSD values of the backbone atoms in the system tend to converge after 7 ns, showing fluctuations of around 1 Å. The low RMSD value during the simulation time indicated that the 3D structural model represents a stable folding conformation.

A number of activity data for A3 adenosine receptor inhibitors, that belong to diverse chemical classes, are currently available. Biological activity data of 121 hA3R antagonists, represented as pKi, were collected from literature [33–39].

All reported A3 receptor antagonists were divided into four groups (Fig. 11): triazolo-quinoxaline (group 1, a); pyrazolo-quinoline (group 2, b and c); annelated triazolo-pyrazine (group 3, d–g); other heterocyclic derivatives (group 4, h–p). The pKi-range of the four groups was homogeneous (group 1: 9.22–5.85; group 2: 8.89–6.26; group 3: 8.89–5.87; group 4: 9.19–6.13) (see supplementary data).

All antagonist structures were docked into TM binding site of the hA3 model using GLIDE [40]. As protein template for docking we used the 20 ns-time snapshot in which the EL2 presents a much more open conformation suitable for the binding of the ligand.

In Fig. 12 docking poses of the most active compound for each group of inhibitors are presented: the triazolo-quinoxaline derivative #40, the pyrazolo-quinoline derivative #5, the annelated triazolo-pyrazine derivative #4, and the heterocyclic derivative #8 (see supplementary data). These four compounds assume an almost identical orientation with the aromatic tricycle on the same plane. With the exception of compound #8 (the heterocycle derivative), all these inhibitors establish H-bond with the binding pocket. Compound #40 of triazolo-quinoxaline group forms two H-bonds, one with Met86 and another with Asn250; among the pyrazolo-quinoline derivatives, compound #5 is H-bonded with Val263; the annelated triazolo-pyrazine derivative #4 forms two H-bonds with Met86.

The resulting docked complexes were imported in PHASE [41] module for the development of 3D quantitative structure–activity relationship (QSAR) Pharmacophore model, and common pharmacophore features were identified and scored. In each group of ligands, the generated pharmacophore hypotheses consisted of four features: one acceptor site (A), and three aromatic ring sites (R). The alignments of all the ligands to the top-ranked pharmacophores were used to generate QSAR models, setting the number of partial least square (PLS) factors from 1 to 6 (Fig. 13).

The datasets of compounds were divided into training and test sets. Two different approaches for splitting the datasets were used. In the first one, training sets were constructed by choosing a percentage (80%) of the total number of compounds in each bin randomly. The other approach is based on Kohonen map-artificial neural network, now more widely called self organizing maps (SOM) [42,43]. Descriptors calculation, and autoscaling of descriptors matrix were the starting point to perform Kohonen clustering approach. The selected test set members are characterized by the minimal distance from the centroid of each cell in the top map.

Predicted activities of training and test set compounds were plotted against their experimental activities, and the relevant

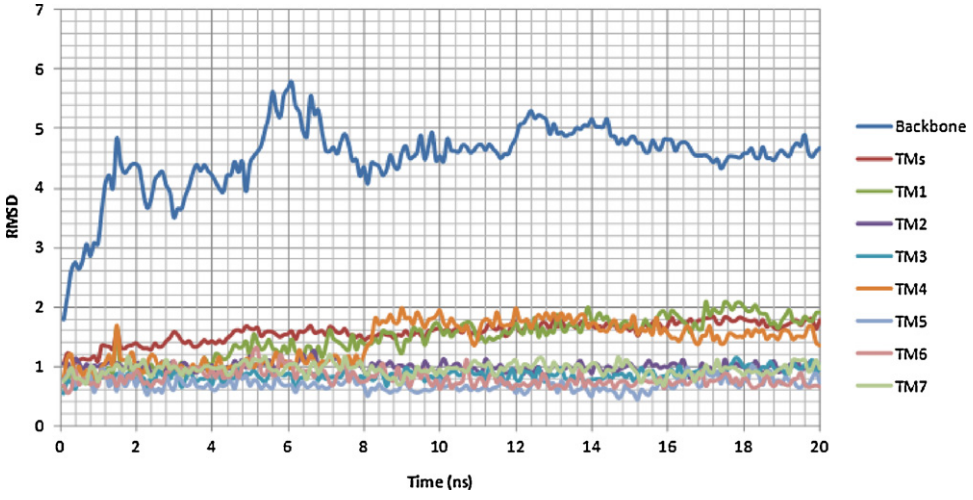

Fig. 8. RMSD of the TMs backbone in function of time.

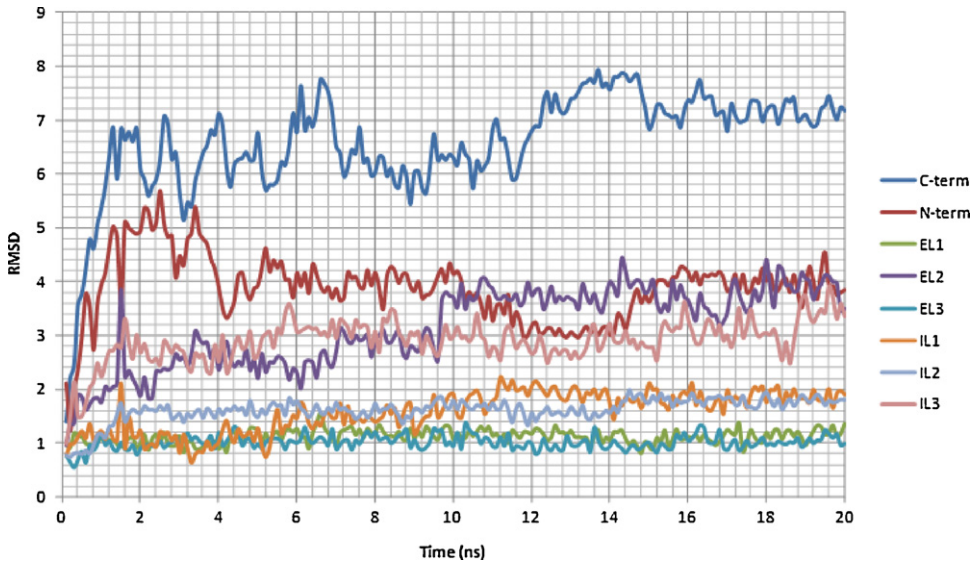

Fig. 9. RMSD of the loops backbone in function of time.

statistics were computed. The Phase statistical analysis for the four groups, labelled as groups 1–4, for each of data set selection method is shown in Tables 5 and 6. A statistical analysis which included the R^2 versus RMSE/SD plot was employed to choose the best PLS model for the different selection methods. The best model was chosen on the basis of PLS factor model minimum observed in RMSE/SD value, with R^2 value still higher than 0.9 and R^2_{pred} higher than 0.5. Only models with good statistical parameters for the training set and exhibiting good predictive ability against test set were chosen.

Group 4 did not exhibit excellent statistical prediction in both methods and therefore was not considered further.

Group 2 exhibited comparatively better PLS statistical qualities and excellent prediction of test set compounds in both selection methods, it showed correlation coefficient (R^2) of 0.96 for random selection of test set, test set prediction (R^2_{pred}) of 0.75 and R-Pearson of 0.95. The low standard deviation (SD) and root-mean-squared error (RMSE) contributes significantly to the model.

Fig. 10. EL2 of the hA3 adenosine receptor before (purple) and after (green) 20 ns of molecular dynamics.

Table 5
3D-QSAR Results summary for random selection (factors = number of factors in the partial least squares regression model; SD = standard deviation; RMSE = root-mean-square error; R^2_{pred} = value of the predicted activity; *R*-Pearson = Pearson *R* value for the correlation between the predicted and observed activity; Δ = difference from preceding).

Factors	SD	R^2	RMSE	R^2_{pred}	*R*-Pearson	RMSE/SD	Δ	Opt. model
Group 1								
1	0.62	0.66	0.52	0.19	0.61	0.84		–
2	0.46	0.82	0.65	0.64	0.85	1.15	0.30	–
3	0.31	0.92	0.38	0.57	0.76	1.21	0.06	√
4	0.20	0.97	0.44	0.42	0.70	2.17	0.96	–
5	0.13	0.99	0.38	0.57	0.79	2.97	0.80	–
6	0.08	0.99	0.38	0.57	0.78	4.52	1.55	–
Group 2								
1	0.56	0.41	0.32	0.69	0.91	0.57		–
2	0.33	0.80	0.34	0.65	0.85	1.01	0.44	–
3	0.26	0.88	0.32	0.69	0.89	1.22	0.21	–
4	0.21	0.93	0.33	0.67	0.88	1.58	0.36	√
5	0.15	0.96	0.29	0.75	0.95	1.87	0.29	–
Group 3								
1	0.61	0.48	0.74	0.10	0.64	1.21		–
2	0.46	0.72	0.58	0.45	0.83	1.26	0.04	–
3	0.35	0.84	0.46	0.65	0.88	1.31	0.05	–
4	0.29	0.90	0.45	0.67	0.91	1.56	0.25	√
Group 4								
1	0.44	0.69	1.03	0.31	0.96	2.34		–
2	0.26	0.90	0.00	0.34	0.96	0.01	−2.33	√
3	0.16	0.96	0.98	0.37	0.97	6.01	6.00	–

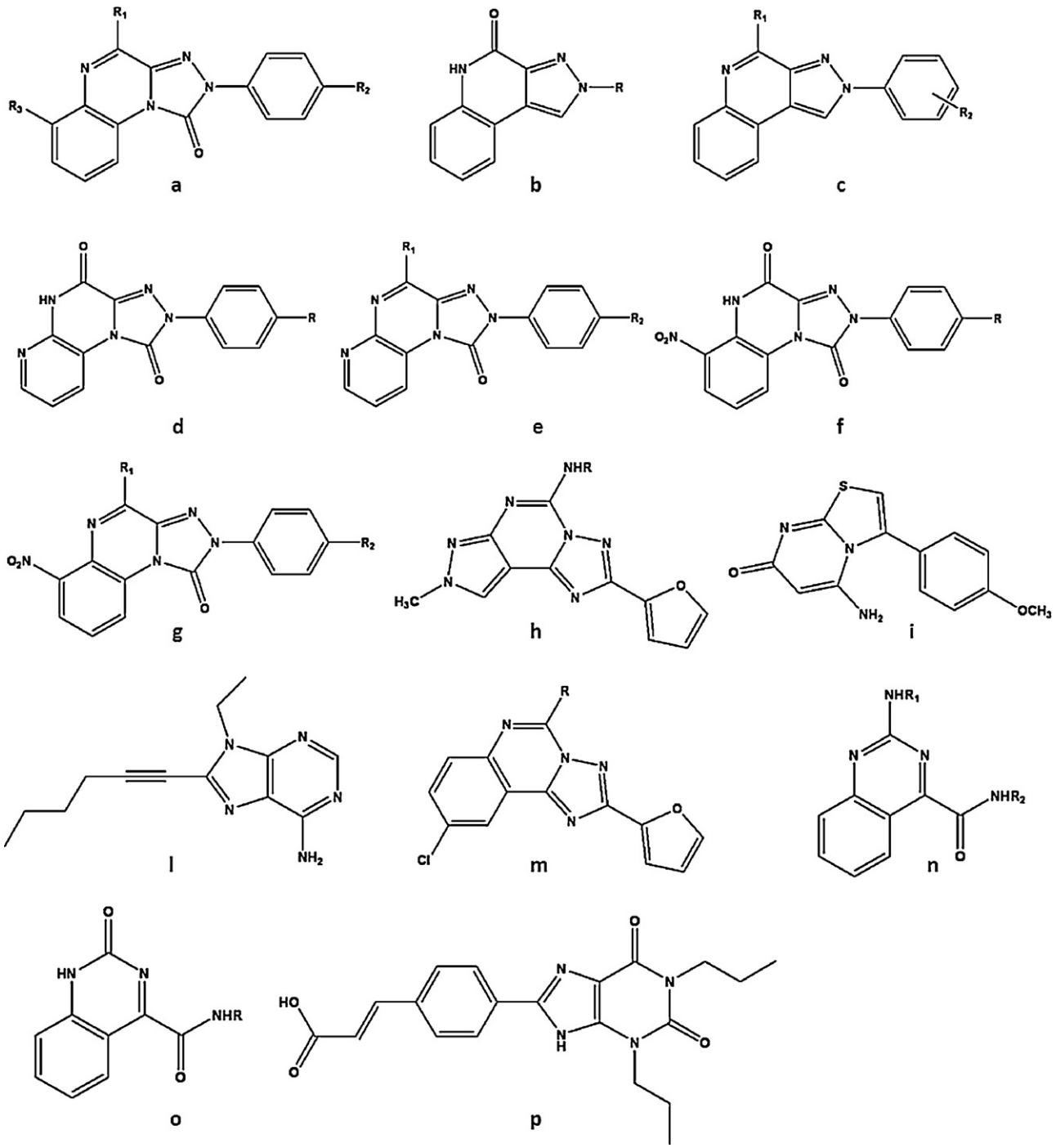

Fig. 11. A3 adenosine receptor inhibitors: triazolo-quinoxaline derivatives (a), pyrazolo-quinoline derivatives (b and c), annelated triazolo-pyrazine derivatives (d–g), heterocyclic derivatives (h–p).

For groups 1–3, the most significant model were obtained for Random selection, because R^2_{pred} for SOM resulted as negative value.

The scatter plot for the training (a) and test set (b) indicates a reasonably good correlation between the predicted and experimental activities (Fig. 14).

The best obtained pharmacophore models were used to retrieve new potential inhibitors from "lead like" ZINC database (3,027,619 compounds) using virtual parallel screening.

Screened molecules were required to match all the hypotheses features. Database hits were ranked in order of their Fitness score, a measure of how well the aligned ligand conformer matches the hypothesis based on site matching, vector alignments and volume terms. As a result, 18189 potential ligand hits, that match all the hypotheses, were identified. Here, we report the ten compounds with the best Fitness score (Table 7); the chemical structures of these hit molecules are presented in Fig. 15.

Therefore, these selected compounds were docked into the binding site of the modeled protein. The conformations of these hits, bound to the modeled A3R, were also analyzed to determine hydrogen-bonding and hydrophobic interactions. The docking results for the final hit molecules are given in Table 8, whereas the binding modes (structures and interacting residues) are shown in Fig. 16.

Table 6
3D-QSAR Results summary for SOM selection (for legend see Table 5).

Factors	SD	R^2	RMSE	R^2_{pred}	*R*-Pearson	RMSE/SD	Δ	Opt. model
Group 1								
1	0.55	0.71	0.99	−0.85	−0.08	1.80	–	–
2	0.38	0.86	1.08	−1.24	−0.20	2.83	1.02	–
3	0.25	0.94	1.02	−1.00	−0.18	4.10	1.27	√
4	0.13	0.99	1.12	−1.37	−0.23	8.70	4.60	–
5	0.08	0.99	1.09	−1.28	−0.19	14.24	5.54	–
6	0.06	1.00	1.09	−1.27	−0.20	18.36	4.12	–
Group 2								
1	0.56	0.42	0.47	0.33	0.60	0.83	–	–
2	0.38	0.75	0.44	0.40	0.70	1.16	0.33	–
3	0.28	0.87	0.28	0.75	0.89	1.02	−0.14	–
4	0.23	0.91	0.27	0.77	0.89	1.17	0.15	√
5	0.18	0.95	0.25	0.81	0.90	1.39	0.22	–
Group 3								
1	0.63	0.46	0.94	−0.19	−0.26	1.48	–	–
2	0.40	0.80	0.83	−0.18	−0.07	2.10	0.62	–
3	0.29	0.90	0.75	0.03	0.25	2.57	0.47	–
4	0.19	0.96	0.84	−0.20	0.08	4.51	1.94	√
Group 4								
1	0.40	0.82	0.62	0.09	0.59	1.55	–	–
2	0.21	0.95	0.69	−0.12	0.54	3.27	1.72	√

The docked models indicate that the ligands maintain key interactions with the TM2, TM3, TM6 and TM7. Another important interaction with EL2 seems to be fundamental.

The drug-like character of the lead compounds was assessed by evaluating their physicochemical properties using QikProp [44]. Their molecular weights were <500 Da; they had <5 hydrogen bond donors and <10 hydrogen bond acceptors, and log*P* values of <5 (Table 9). These properties are all well within the acceptable range of Lipinski's rule of five.

The pharmacokinetic parameters of the molecules (ADMET) showed that the partition coefficient (QPlogPo/w) and water solubility (QPlogS) values, which are crucial for estimating the absorption and distribution of drugs within the body, ranged approximately from 1.81 to 3.32 and from −5.01 to −3.56, respectively. Thus the pharmacokinetic parameters are well within the acceptable range defined for human use, thereby indicating the potential drug-likeness of these molecules. The structure selected by our proposed screening procedure could serve as potential specific inhibitors against the A3 human receptor and therefore could be potentially used for therapeutic treatments of cancer.

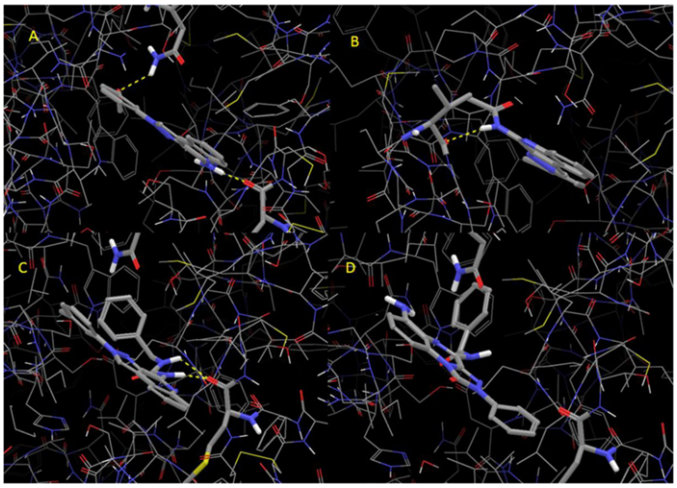

Fig. 12. Representative antagonists structures docked into TM binding site of hA3. (A) Compound #40 of triazolo-quinoxaline group, (B) compound #5 of pyrazolo-quinoline group, (C) compound #4 of annelated triazolo-pyrazine group, (D) compound #8 of heterocyclic derivatives group.

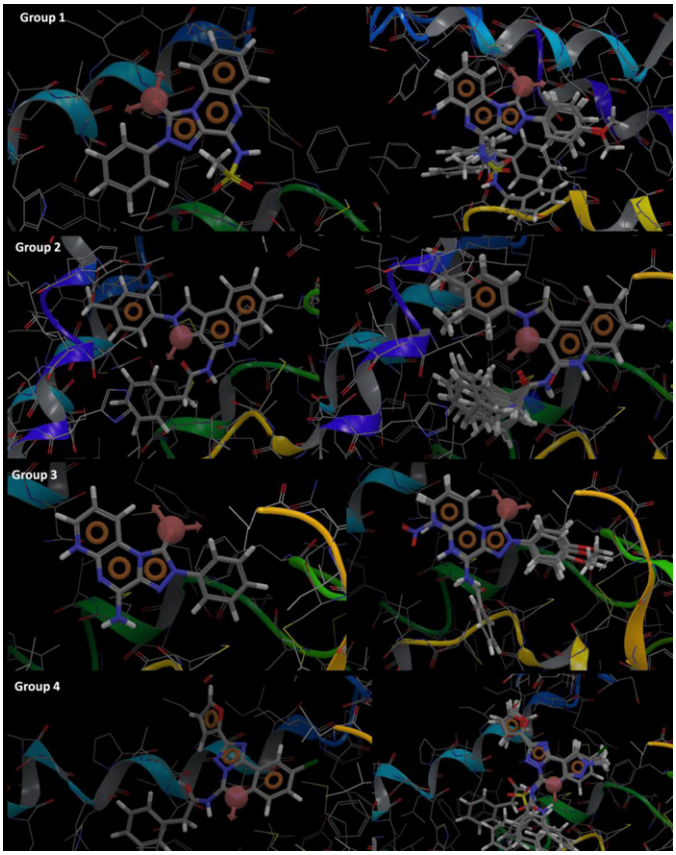

Fig. 13. Pharmacophore mapping of the most active compound (left); superimposition of active compounds with the pharmacophore.

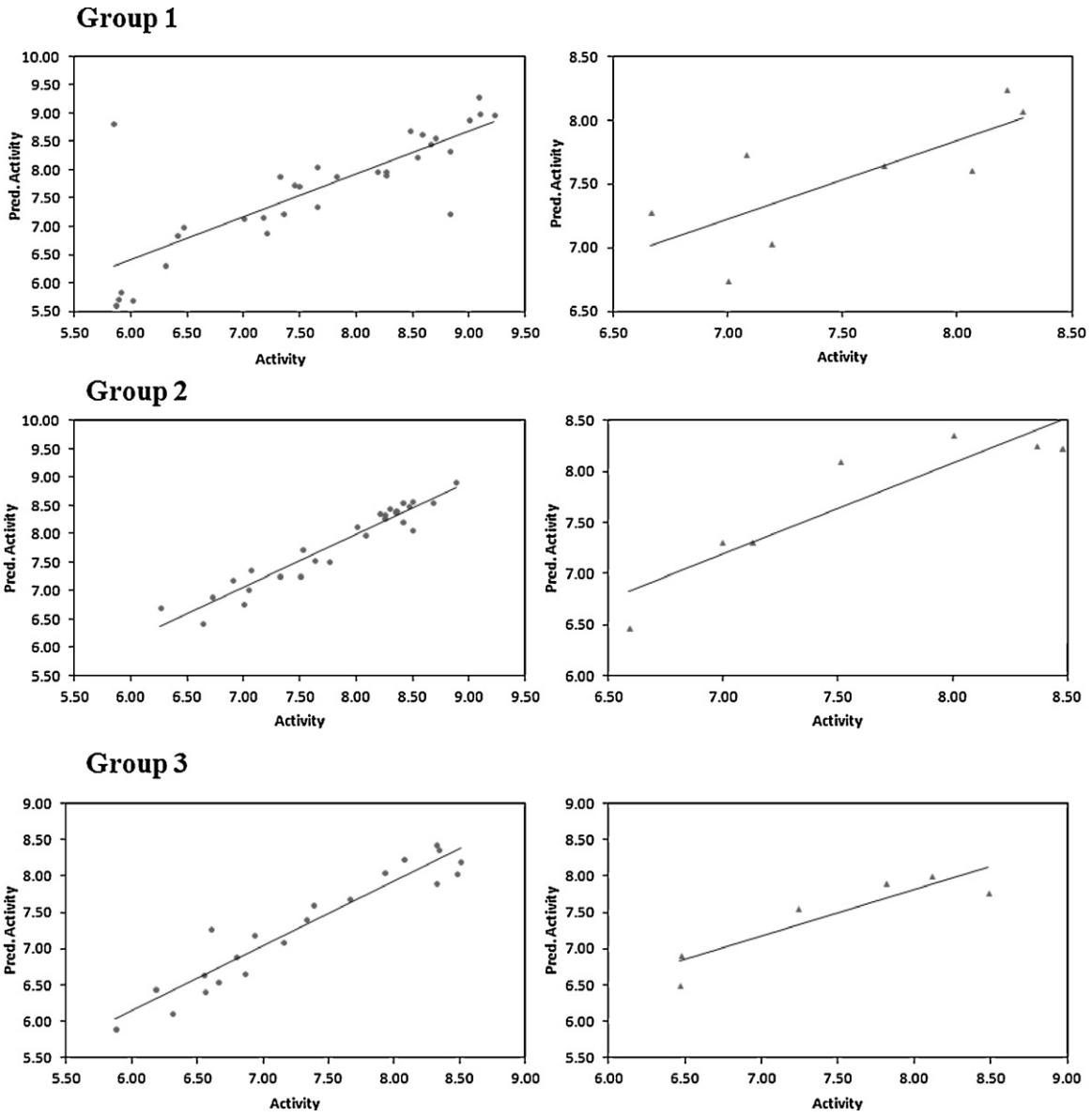

Fig. 14. Scatter plots with best fit for the hA3R QSAR models applied to the training set (a) and the test set (b).

3. Computational methods

3.1. Model building

The amino acid sequence of human A3R, consisting of 318 units, was retrieved from Uniprot (P33765). Crystallography structure of the bovine rhodopsin (PDB ID: 1U19) and of the human A2A adenosine receptor (PDB ID: 3EML) were selected as template proteins. 3D models were constructed from the sequence alignment between FASTA sequence of the protein and the template proteins using LOMETS [27]. In order to assess the reliability of the modeled structure of A3R, the root mean square deviation (RMSD) was

Table 7
Fitness score of the identified lead.

Zinc ID	Model group 1		Model group 2		Model group 3	
	Fitness	Pred pKi	Fitness	Pred pKi	Fitness	Pred pKi
978790	2.268	7.75	1.439	7.09	1.495	6.89
3192107	2.455	7.59	1.802	7.44	2.514	7.25
6624316	2.458	7.80	1.695	8.00	2.536	7.37
6624541	2.459	7.77	1.696	8.04	2.540	7.53
8578947	2.460	7.63	1.719	7.25	2.463	7.07
13363145	2.473	7.67	1.705	7.37	2.423	7.29
20085946	2.493	7.60	1.696	7.41	2.577	7.03
21774670	2.463	8.24	1.574	7.51	2.476	7.42
21774675	2.447	7.84	1.540	7.73	2.507	7.47
21774724	2.468	7.66	1.551	7.48	2.515	7.33

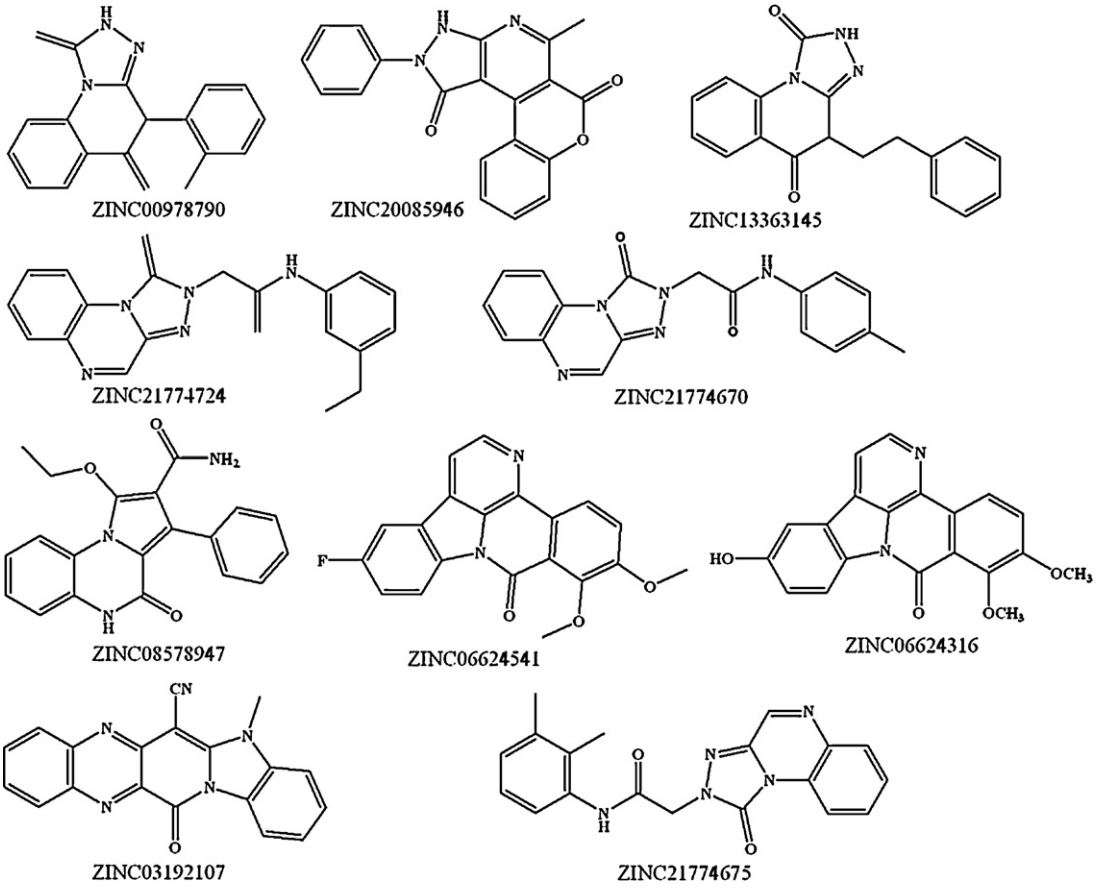

Fig. 15. Chemical structures of ten compounds with the best Fitness score.

Table 8
Extra Precision (XP) Glide results for the ten lead molecules.

Zinc ID	Fitness	GScore	Amino acids involved in hydrophobic interactions	Amino acids involved in H-bond
978790	2.518	−6.549	V72, F168, M177, L264, I268	M86
3192107	2.455	−6.606	V72, M86, F168, I253, V263, L264, I268	
6624316	2.458	−7.434	V72, L89, L90, L91, M177, L246, I253, V259, I263, L264, I268	T94
6624541	2.459	−7.39	V72, M86, F168, M177, L246, I253, V263, L264	N250
8578947	2.46	−7.298	V72, M86, F168, I253, V263, L264	S73
13363145	2.473	−6.927	V72, L90, L91, M177, L246, I253, V259, L264, I268	M86, L90
20085946	2.493	−7.415	V72, M86, L90, F168, M177, V259, L264, I268	M86
21774670	2.463	−8.427	V72, M86, L90, L91, P168, M177, L246, I268	M86, N250
21774675	2.447	−8.461	V72, M86, L90, L91, F168, M177, L246, I268	M86
21774724	2.468	−8.983	V72, M86, L89, L90, L91, C166, F168, M177, L246, I268	M86

Table 9
QikProp properties of the identified hits (MW = molecular weight; HBD = hydrogen bond donors; HBA = hydrogen bond acceptors; QPlogPo/w = predicted octanol/water partition coefficient logP; QPlogS = predicted aqueous solubility S in mol/L; QPP Caco = predicted apparent Caco-2 cell permeability in nm/s; QPPMDC = predicted apparent MDCK cell permeability in nm/s).

Zinc ID	MW	HBD	HBA	QPlogPo/w	QPlogS	Percent human oral absorption	QPP Caco	QPP MDCK
978790	292.29	1	6	1.8	−3.62	85.55	483.06	225.31
3192107	325.32	0	6.5	2.07	−4.25	89.99	697.98	335.4
6624316	346.34	1	6.25	2.56	−3.58	96.61	1128.89	563.97
6624541	348.33	0	5.5	3.32	−3.89	100	3874.95	3860.24
8578947	347.37	3	5	2.8	−4.51	90.16	412.81	190.12
13363145	306.32	1	6	2.16	−3.56	87.81	493.54	230.6
20085946	343.34	1	7.5	2.0	−3.81	90.84	822.44	400.49
21774670	333.34	1	6.5	2.68	−4.54	94.12	751.26	363.16
21774675	347.37	1	6.5	3.06	−5.08	96.97	814.51	396.31
21774724	347.37	1	6.5	2.99	−4.83	95.97	754.89	365.05

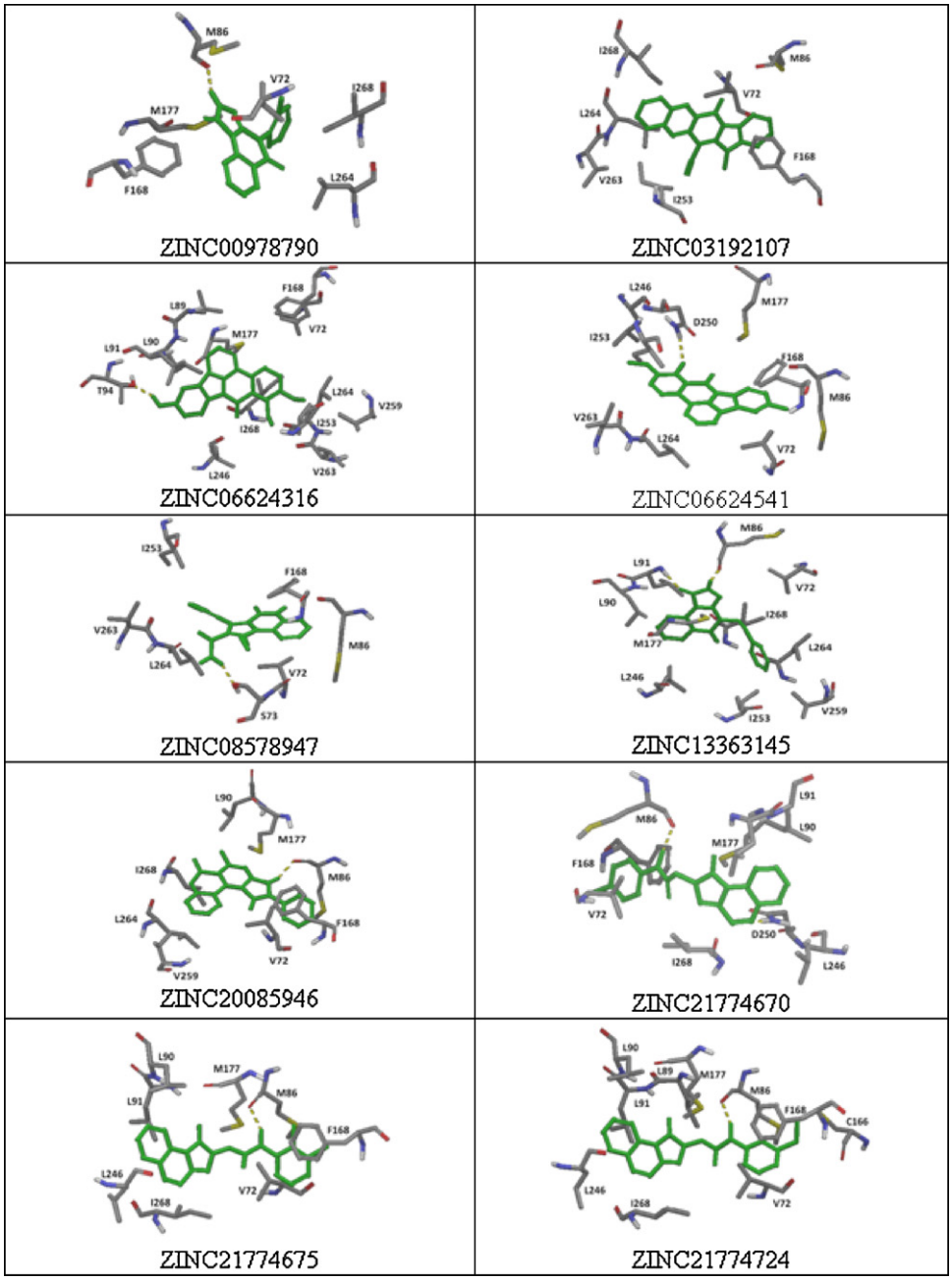

Fig. 16. Binding poses of the ten lead molecules. Hydrogen bonds are shown as dotted yellow lines.

calculated by superimposing it on the template structures. The backbone conformation of the modeled structure was calculated by analyzing the phi (Φ) and psi (ψ) torsion angles using PROCHECK [30], as determined by Ramachandran plot statistics.

3.2. Molecular dynamics simulation

The stability of the modeled A3R was checked in a 20 ns molecular dynamics (MD) simulation using Desmond [32]. The model was first immerged into a lipid bi-layer; membrane orientation was taken from OPM (Orientations of Proteins in Membranes) database [45]. The system was the solvatated with a cubic box of water molecules (SPC water model), and was first relaxed using the Desmond relaxation model. The completed equilibration run was followed by a production run performed with NPT conditions using the Berendsen thermostat [46] (300 K and 1.103 bar).

3.3. Molecular docking

Glide software [40] was used to perform the molecular docking of the known inhibitors and retrieved hits into the hA3R model. This program uses a hierarchical series of filters to search for possible locations of the ligand in the active-site region of the receptor, while the shape and properties of the receptor are represented on a grid by several sets of fields that progressively provide more accurate scoring of the ligand poses. An extensive conformational search is performed using a heuristic screen that rapidly eliminates unsuitable conformations (e.g. long-range internal H-bonds or sterical clashes). The entire amount of poses generated is then

hierarchically classified, refined and further minimized into the active site grid before being finally scored using the proprietary GlideScore function, defined as in Eq. (1).

$$\text{GScore} = 0.065 \times \text{vdW} + 0.130 \times \text{Coul} + \text{Lipo} + \text{Hbond} + \text{Metal} + \text{BurryP} + \text{RotB} + \text{Site} \quad (1)$$

where:

vdW is the van der Waals energy term, Coul is the Coulomb energy,
Lipo is a Lipophilic contact term which rewards favourable hydrophobic interactions,
Hbond is a H-bonding term,
Metal is a metal-binding term (where applicable),
BuryP is a penalty term applied to buried polar groups,
RotB is a penalty for freezing rotatable bonds,
Site is a term used to describe favourable polar interactions in the active site.

Our experiments were carried out using the default parameters and the following protocol: initially, the Standard Precision (SP) level of accuracy was used for the generation and scoring of 10 poses for each ligand. The top-scored conformation was further re-docked using the Extra-Precision (XP) algorithm. Finally the best poses were refined using the "Refine" option (this performs an optimization of the ligand structure in the field of the receptor) at the XP level of accuracy. The Extra-Precision mode combines a powerful sampling protocol with the use of a custom scoring function designed to identify ligand poses that would be expected to have unfavourable energies. The presumption is that only active compounds will have available poses that avoid these penalties and receive favourable scores for appropriate hydrophobic contact between the protein and the ligand. The XP sampling method is based on an anchor and refined growth strategy: anchor fragments of the docked ligand (typically rings) are chosen from the set of SP poses and the molecule is re-grown bond by bond from these anchor positions; a complete minimization and XP scoring cycle is carried out on the large ensemble of poses generated by growing method. The XP scoring functions integrates the basic GlideScore functions with additional terms: to model solvation an explicit water term is used, parameterized on several known protein–ligand complexes; similarly, additional parameterized rewards are calculated for buried hydrophobic pockets occupied by hydrophobic ligand groups.

3.4. Pharmacophore mapping and 3D-QSAR method

A dataset of 121 derivatives was used in the present study. The dataset has been chosen in order to cover the information about its activity against A3R, data reported as Ki values, converted to pKi. Common pharmacophores containing four sites were generated with PHASE, with the requirement that all actives match. Scoring with respect to actives was conducted using default parameters for site, vector, and volume terms. The best hypotheses were selected on the basis of the fitness score and other relevant results such as survival score, posthoc score and survival minus inactive score, which ensure their feasibility. Generated hypotheses with the aligned conformations were combined with known activity data to create a 3D-QSAR model that identifies overall aspects of molecular structure that govern activity. The developed 3D-QSAR model was externally validated and cross validated using partial least square equations.

3.5. ADME virtual prediction

The QikProp program [44] was used to obtain the ADME properties of the compounds. It predicts both physically significant descriptors and pharmaceutically relevant features, such as principal descriptors and physiochemical properties. It also evaluated the drug-like acceptability of the compounds, based on Lipinski's rule of five, essential for rational drug design.

4. Conclusion

Four adenosine receptor subtypes (A1, A2A, A2B, and A3) have been cloned and pharmacologically characterized, all of them are G protein-coupled receptors. The new structure of hA2A, solved in 2008, provided a new starting point for homology modelling and was used as template to built model of hA3 adenosine receptor. The inclusion of an explicit lipid bilayer into the energy minimization simulation helped to optimize the structure quality. Our theoretical model of hA3 adenosine receptor was used to evaluate and quantify the structure-activity relationships of known antagonists. Later, the 3D-QSAR model was used with the purpose of identifying new potential inhibitors for A3R. The identified hits could be potential inhibitors for the desired target receptor.

Appendix A. Supplementary data

Supplementary data associated with this article can be found, in the online version, at http://dx.doi.org/10.1016/j.jmgm.2013.03.001.

References

[1] M.P. Abbracchio, R. Brambilla, S. Ceruti, H.O. Kim, D.K.J.E. Von Lubitz, K.A. Jacobson, F. Cattabeni, G protein-dependent activation of phospholipase C by adenosine A3 receptors in rat brain, Molecular Pharmacology 48 (1995) 1038–1045.
[2] B.B. Fredholm, A.P. Ijzerman, K.A. Jacobson, K.N. Klotz, J. Linden, Interational Union of Pharmacology 2001: XXV. Nomenclature and classification of adenosine receptors, Pharmacological Reviews 53 (2001) 527–552.
[3] R. Yaar, M.R. Jones, J.F. Chen, K. Ravid, Animal models for the study of adenosine receptor function, Journal of Cellular Physiology 202 (2005) 9–20.
[4] S. Gessi, E. Cattabriga, A. Avitabile, R. Gafà, G. Lanza, L. Cavazzini, N. Bianchi, R. Gambari, C. Feo, A. Liboni, S. Gullini, E. Leung, S. Mac-Lennan, P.A. Borea, Elevated expression of A3 adenosine receptors in human colorectal cancer is reflected in peripheral blood cells, Clinical Cancer Research 10 (2004) 5895–5901.
[5] A. Lauria, I. Abbate, C. Patella, A. Martorana, G. Dattolo, A.M. Almerico, New annelated thieno[2,3-e][1,2,3]triazolo[1,5-a]pyrimidines, with potent anticancer activity, designed through VLAK protocol, European Journal of Medicinal Chemistry 62 (2013) 416–424.
[6] A. Lauria, C. Patella, I. Abbate, A. Martorana, A.M. Almerico, Lead optimization through VLAK protocol: New annelated pyrrolo-pyrimidine derivatives as antitumor agents, European Journal of Medicinal Chemistry 55 (2012) 375–383.
[7] A.M. Almerico, M. Tutone, A. Lauria, Molecular dynamics studies on Mdm2 complexes: an analysis of the inhibitor influence, Biochemical and Biophysical Research Communications 424 (2012) 341–347.
[8] A.M. Almerico, M. Tutone, A. Lauria, Receptor-guided 3D-QSAR approach for the discovery of c-kit tyrosine kinase inhibitors, Journal of Molecular Modeling 18 (2012) 2885–2895.
[9] M. Tutone, A. Lauria, A.M. Almerico, Study of the role of gatekeeper mutations V654A and T670I of c-kit kinase in the interaction with inhibitors by means mixed molecular dynamics/docking approach, Bioinformation 7 (2011) 296–298.
[10] A. Lauria, M. Tutone, A.M. Almerico, Virtual lock-and-key approach: the in silico revival of Fischer model by means of molecular descriptors, European Journal of Medicinal Chemistry 46 (2011) 4274–4280.
[11] A.M. Almerico, M. Tutone, A. Lauria, 3D-QSAR pharmacophore modeling and in silico screening of new Bcl-xl inhibitors, European Journal of Medicinal Chemistry 45 (2010) 4774–4782.
[12] A. Lauria, M. Ippolito, M. Fazzari, M. Tutone, F. Di Blasi, F. Mingoia, A.M. Almerico, IKK-ß inhibitors: an analysis of drug–receptor interaction by using molecular docking and pharmacophore 3D-QSAR approaches, Journal of Molecular Graphics and Modelling 29 (2010) 72–81.
[13] A. Lauria, M. Ippolito, A.M. Almerico, Principal component analysis on molecular descriptors as an alternative point of view in the search of new Hsp90 inhibitors, Computational Biology and Chemistry 33 (2009) 386–390.
[14] A.M. Almerico, M. Tutone, A. Lauria, In-silico screening of new potential Bcl-2/Bcl-xl inhibitors as apoptosis modulators, Journal of Molecular Modeling 15 (2009) 349–355.

[15] A. Lauria, M. Ippolito, A.M. Almerico, Combined use of PCA and QSAR/QSPR to predict the drugs mechanism of action. An application to the NCI ACAM database, QSAR and Combinational Science 28 (2009) 387–395.
[16] A. Lauria, M. Ippolito, A.M. Almerico, Inside the Hsp90 inhibitors binding mode through induced fit docking, Journal of Molecular Graphics and Modelling 27 (2009) 712–722.
[17] D.M. Perez, S.S. Karnik, Multiple signaling states of G-protein-coupled receptors, Pharmacological Reviews 57 (2005) 147–161.
[18] M. Klinger, M. Freissmuth, C. Nanoff, Adenosine receptors: G protein-mediated signalling and the role of accessory proteins, Cellular Signalling 14 (2002) 99–108.
[19] K. Palezewski, T. Kumasaka, T. Hori, C.A. Behnke, H. Motoshima, B.A. Fox, I. Le Trong, D.C. Teller, T. Okada, R.E. Stenkamp, M. Yamamoto, M. Miyano, Crystal structure of rhodopsin: a G protein-coupled receptor, Science 289 (2000) 739–745.
[20] F. Fanelli, P.G. De Benedetti, Inactive and active states and supramolecular organization of GPCRs: insights from computational modeling, Journal of Computer-Aided Molecular Design 20 (2006) 449–461.
[21] V. Jaakola, M.T. Griffith, M.A. Hanson, V. Cherezov, E.Y.T. Chien, J.R. Lane, A.P. Ijzerman, R.C. Stevens, The 2.6 Angstrom crystal structure of a human A2A adenosine receptor bound to an antagonist, Science 322 (2008) 1211–1217.
[22] V. Cherezov, D.M. Rosenbaum, M.A. Hanson, S.G. Rasmussen, F.S. Thian, T.S. Kobilka, H.J. Choi, P. Kuhn, W.I. Weis, B.K. Kobilka, R.C. Stevens, High-resolution crystal structure of an engineered human beta2-adrenergic G protein-coupled receptor, Science 318 (2007) 1258–1265.
[23] A. Warne, M.J. Serrano-Vega, J.G. Baker, R. Moukhametzianov, P.C. Edwards, R. Henderson, A.G.W. Leslie, C.G. Tate, G.F. Schertler, Structure of a beta1-adrenergic G-protein-coupled receptor, Nature 454 (2008) 486–491.
[24] T. Okada, M. Sugihara, A.N. Bondar, M. Elstner, P. Entel, V. Buss, The retinal conformation and its environment in rhodopsin in light of a new 2.2 A crystal structure, Journal of Molecular Biology 342 (2004) 571–583.
[25] F.G. Sajjadi, G.S. Firestein, cDNA Cloning and sequence analysis of the human A3 adenosine receptor, Biochimica et Biophysica Acta 1179 (1993) 105–107.
[26] C.A. Salvatore, M.A. Jacobson, H.E. Taylor, J. Linden, R.G. Johnson, Molecular cloning and characterization of the human A3 adenosine receptor, Proceedings of the National Academy Science of the United States of America 90 (1993) 10365–10369.
[27] S. Wu, Y. Zhang, A local meta-threading-server for protein structure prediction, Nucleic Acids Research 35 (2007) 3375–3382.
[28] A. Fiser, A. Sali, ModLoop: automated modeling of loops in protein structures, Bioinformatics 19 (2003) 2500–2501.
[29] P. Benkert, M. Künzli, T. Schwede, QMEAN server for protein model quality estimation, Nucleic Acids Research 37 (2009) 510–514.
[30] R.A. Laskowski, M.W. MacArthur, D.S. Moss, J.M. Thornton, PROCHECK: a program to check the stereochemical quality of protein structures, Journal of Applied Crystallography 26 (1993) 283–291.
[31] H. Frauenfelder, S.G. Sligar, P.G. Wolynes, The energy landscapes and motions of proteins, Science 254 (1991) 1598–1603.
[32] Desmond Molecular Dynamics System, version 2.2, 2009, D.E. Shaw Research, New York, NY. Maestro-Desmond Interoperability Tools, version 2.2, Schrödinger, LLC, New York, NY, 2009.
[33] V. Colotta, D. Catarzi, F. Varano, R. Calabri, O. Lenzi, G. Filacchioni, G. Martini, L. Trincavelli, F. Deflorian, S. Moro, 1,2,4-triazolo[4,3-a]quinoxalin-1-one moiety as an attractive scaffold to develop new potent and selective human A3 adenosine receptor antagonists: Synthesis, pharmacological, and ligand-receptor modeling studies, Journal of Medicinal Chemistry 47 (2004) 3580–3590.
[34] O. Lenzi, V. Colotta, D. Catarzi, F. Varano, G. Filacchioni, C. Martini, L. Trincavelli, O. Ciampi, K. Varani, F. Marighetti, E. Morizzo, S. Moro, 4-Amido-2-aryl-1,2,4-triazolo[4,3-a]quinoxalin-1-ones as new potent and selective human A3 adenosine receptor antagonists. Synthesis, pharmacological evaluation, and ligand-receptor modeling studies, Journal of Medicinal Chemistry 49 (2006) 3916–3925.
[35] V. Colotta, D. Catarzi, F. Varano, O. Lenzi, G. Filacchioni, G. Martini, L. Trincavelli, O. Ciampi, C. Traini, A.M. Pugliese, F. Pedata, E. Morizzo, S. Moro, Synthesis, ligand–receptor modeling studies and pharmacological evaluation of novel 4-modified-2-aryl-1,2,4-triazolo[4,3-a] quinoxalin-1-one derivatives as potent and selective human A3 adenosine receptor antagonists, Bioorganic and Medicinal Chemistry 16 (2008) 6086–6102.
[36] V. Colotta, D. Catarzi, F. Varano, F. Capelli, O. Lenzi, G. Filacchioni, G. Martini, L. Trincavelli, O. Ciampi, A.M. Pugliese, F. Pedata, A. Schiesaro, E. Morizzo, S. Moro, New 2-arylpyrazolo[3,4-c]quinoline derivatives as potent and selective human A3 adenosine receptor antagonists. Synthesis, pharmacological evaluation, and ligand-receptor modeling studies, Journal of Medicinal Chemistry 50 (2007) 4061–4076.
[37] E. Morizzo, F. Capelli, O. Lenzi, D. Catarzi, F. Varano, G. Filacchioni, F. Vincenzi, K. Varani K., P. Borea, V. Colotta, S. Moro, Scouting Human A3 Adenosine Receptor Antagonist Binding Mode Using a Molecular Simplification Approach: From Triazoloquinoxaline to a Pyrimidine Skeleton as a Key Study, Journal of Medicinal Chemistry 50 (2007) 6596–6606.
[38] C. Bolcato, C. Cusan, G. Pastorin, G. Spalluto, B. Cacciari, K.N. Klotz, E. Morizzo, S. Moro, Pyrazolo-triazolo-pyrimidines as adenosine receptor antagonists: Effect of the N-5 bond type on the affinity and selectivity at the four adenosine receptor subtypes, Purinergic Signalling 4 (2008) 39–46.
[39] Y.C. Kim, X. Ji, K.A. Jacobson, Derivatives of the triazoloquinazoline adenosine antagonists (CGS 15943) are selective for the human A3 receptor subtype, Journal of Medicinal Chemistry 39 (1996) 4142–4148.
[40] Glide, version 5.7, Schrödinger, LLC, New York, NY, 2012.
[41] Phase, version 3.1, Schrödinger, LLC, New York, NY, 2009.
[42] J. Zupan, M. Novic, I. Ruisánchez, Kohonen and counterpropagation artificial neural networks in analytical chemistry, Chemometrics and Intelligent Laboratory Systems 38 (1997) 1–23.
[43] J. Gasteiger, J. Zupan, Neural networks in chemistry, Angewandte Chemie International English Edition 32 (1993) 503–527.
[44] QikProp, version 3.2, Schrödinger, LLC, New York, NY, 2009.
[45] M.A. Lomize, A.L. Lomize, I.D. Pogozheva, H.I. Mosberg, OPM: orientations of proteins in membranes database, Bioinformatics 22 (2006) 623–625.
[46] H.J.C. Berendsen, J.P.M. Postma, W.F. van Gunsteren, A. Di Nola, J.R. Haak, Molecular dynamics with coupling to an external bath, Journal of Chemical Physics 81 (1984) 3684–3690.